Patient-specific, multiscale modelling of neointimal hyperplasia in lower-limb vein grafts using readily available clinical data

Journal of Biomechanics 177 (2024) 112428

Contents lists available at ScienceDirect

Journal of Biomechanics

journal homepage: www.elsevier.com/locate/jbiomech

Patient-specific, multiscale modelling of neointimal hyperplasia in lower-limb vein grafts using readily available clinical data

Federica Ninno [a,b], Claudio Chiastra [c], Francesca Donadoni [d], Alan Dardik [e,f,g], David Strosberg [f,g], Edouard Aboian [f], Janice Tsui [h,i], Stavroula Balabani [b,d], Vanessa Díaz-Zuccarini [b,d,*]

[a] Department of Medical Physics and Biomedical Engineering, University College London, London, UK
[b] UCL Hawkes Institute, University College London, London, UK
[c] PolitoBIOMed Lab, Department of Mechanical and Aerospace Engineering, Politecnico di Torino, Turin, Italy
[d] Department of Mechanical Engineering, University College London, London, UK
[e] Vascular Biology and Therapeutics, Yale University School of Medicine, New Haven, CT, USA
[f] Division of Vascular Surgery and Endovascular Therapy, Department of Surgery, Yale University School of Medicine, New Haven, CT, USA
[g] Department of Surgery, VA Connecticut Healthcare Systems, West Haven, CT, USA
[h] Department of Vascular Surgery, Royal Free Hospital NHS Foundation Trust, London, UK
[i] Division of Surgery & Interventional Science, Department of Surgical Biotechnology, Faculty of Medical Sciences, University College London, London, UK

ARTICLE INFO

Keywords:
Computational multiscale modelling
Continuum models
Peripheral arterial disease
Neointimal hyperplasia
Vein grafts

ABSTRACT

The prediction of neointimal hyperplasia (NIH) growth, leading to vein graft failure in lower-limb peripheral arterial disease (PAD), is hindered by the multifactorial and multiscale mechanobiological mechanisms underlying the vascular remodelling process. Multiscale *in silico* models, linking patients' hemodynamics to NIH pathobiological mechanisms, can serve as a clinical support tool to monitor disease progression. Here, we propose a new computational pipeline for simulating NIH growth, carefully balancing model complexity/inclusion of mechanisms and readily available clinical data, and we use it to predict NIH growth for an entire vein graft. To this end, three different fittings to published *in vitro* data of time-averaged wall shear stress (TAWSS) vs nitric oxide (NO) production were tested for predicting long-term graft response (10-month follow-up) on a single patient. Additionally, the sensitivity of the model's predictions to different inflow boundary conditions (BCs) was assessed. The main findings indicate that: (i) a TAWSS-NO hyperbolic relationship best predicts long-term graft response; (ii) the model is insensitive to the inflow BCs if the waveform shape and the systolic acceleration time are comparable with the one acquired at the same time as the computed-tomography scan. This proof-of-concept study demonstrates the potential of using multiscale, computational techniques to predict NIH growth in lower-limb vein grafts, considering the routine clinical scenario of non-standardised data collection and sparse, incomplete datasets.

1. Introduction

Peripheral arterial disease (PAD) is a progressive pathology, characterised by the build-up of lipid-rich plaque, gradually reducing blood flow in the lower limbs (Criqui et al., 2021). Bypass surgery using an autogenous vein – e.g. saphenous vein graft – has been the clinical standard and the most durable revascularisation procedure for patients with severe manifestations of lower extremity PAD (Lu et al., 2014; Muto et al., 2010). Nevertheless, 30–50 % of saphenous vein grafts fail – i.e. they occlude or develop significant restenosis (Owens et al., 2015) – from 1 to 18 months post-intervention (Owens, 2010). This period is the most active from a biological viewpoint (Owens, 2010). Lumen re-narrowing is caused by aggressive neointimal growth, referred to as neointimal hyperplasia (NIH), characterised by exacerbated smooth muscle cells (SMCs) activity (Chaabane et al., 2013). The cause of this phenomenon and why some patients develop clinical restenosis (≥50 % vessel diameter reduction (Singh et al., 2004)) at seemingly indiscriminate timescales is not yet fully understood. The biological complexity

* Corresponding author at: Department of Mechanical Engineering, University College London, Torrington Place, WC1E 7JE London, UK.
E-mail addresses: federica.ninno.20@ucl.ac.uk (F. Ninno), claudio.chiastra@polito.it (C. Chiastra), alan.dardik@yale.edu (A. Dardik), david.strosberg@yale.edu (D. Strosberg), edouard.aboian@yale.edu (E. Aboian), janice.tsui@ucl.ac.uk (J. Tsui), s.balabani@ucl.ac.uk (S. Balabani), v.diaz@ucl.ac.uk (V. Díaz-Zuccarini).

https://doi.org/10.1016/j.jbiomech.2024.112428
Accepted 9 November 2024
Available online 13 November 2024

and multifactorial nature of NIH growth makes it an excellent candidate for the use of multiscale *in silico* models, accounting for a complex network of components interacting at different spatial and temporal scales (Gosak et al., 2018; Walpole et al., 2013).

Multiscale *in silico* models can be divided into equation- and agent-based (ABM) models and have been developed for several vascular adaptation processes in different vascular regions, as reported by (Corti et al., 2021). Equation-based models are *usually* deterministic, continuum models based on systems of ordinary and/or partial differential equations. These models have been broadly implemented to describe the transport of molecular proatherogenic species (Silva et al., 2020) and evaluate the mechanical behaviour or the fluid dynamics at the tissue/organ scale (Chiastra et al., 2021a, 2021b; Colombo et al., 2021a, 2021b). ABMs incorporate stochasticity and are commonly adopted to model the cell-tissue level more realistically (Corti et al., 2021; Hwang et al., 2009). ABMs can be coupled with continuum models (Corti et al., 2021), which allow the computation of near-wall hemodynamic indices – such as time-averaged wall shear stress (TAWSS) – that have been linked to restenosis progression (Ninno et al., 2023). The applicability of ABMs in clinical practice is limited by high computational costs and the availability of information regarding molecular intracellular pathways (Corti et al., 2022b), which is not routinely collected. In this context, parsimonious, multiscale continuum models solely relying on available clinical data for PAD – such as computed tomography (CT) scans and Doppler ultrasound (DUS) images – represent a valid possible alternative.

In our previous work (Donadoni et al., 2017), we developed an equation-based model of the biological mechanisms leading to NIH growth in lower-limb vein grafts. These mechanisms (i.e., SMCs and collagen turnover, growth factors and nitric oxide (NO) production), were described by ordinary differential equations and linked to TAWSS. This hemodynamic metric was obtained from computational fluid dynamics (CFD) analyses, starting from patients' CT and DUS imaging data. The model's output was the three-dimensional (3D) vessel geometry at the desired follow-up. The study demonstrated an overall agreement between the locations of simulated NIH development and those observed in clinical data. Nevertheless, the model presented some limitations. The baseline geometry prior to restenosis was obtained by virtually eliminating the NIH, and only severely stenosed regions were compared against the geometry reconstructed from the CT scan at that specific follow-up. A linear relationship between TAWSS and NO production was assumed, although *in vitro* results suggested that other fitting functions (i.e., hyperbolic and sigmoidal) might better match the data (Andrews et al., 2010). Furthermore, the sensitivity of the model to different inlet boundary conditions (BCs) was not examined. This aspect is crucial as inflow conditions need to be derived from DUS images, often acquired at different time points from the CT scan (Ninno et al., 2024), due to fragmented datasets and unsystematic clinical data collection. Practically, this discrepancy implies that computed TAWSS values for a particular graft do not reflect the patient's hemodynamic condition at that time, potentially resulting in misleading predictions.

In view of the above, in the present study we propose a new, proof-of-concept computational pipeline for predicting neointimal hyperplasia growth along vein grafts, based on readily available clinical data. First, we refined the aforementioned model (Donadoni et al., 2017) by employing different relationships (i.e., linear, hyperbolic and sigmoidal) between TAWSS and NO production based on established *in vitro* experiments (Andrews et al., 2010). We identified the relationship that provides the best NIH predictions for long-term vein graft response on one patient (10-month follow-up). Second, we analysed the influence of different applied inlet BCs – extracted from DUS images acquired at different time points than the CT scan – on restenosis prediction results. Unlike (Donadoni et al., 2017), no virtual NIH removal was needed due to available baseline CT scans, and the model's performance was evaluated along the entire graft rather than selected locations.

2. Methods

Fig. 1 depicts our computational workflow, which is structured into three modules: (i) vessel reconstruction and patient-specific CFD module: blood flow simulations and TAWSS calculations are performed along the whole vein graft on the baseline geometry; (ii) remodelling module: estimated TAWSS values are used as input to a biochemical model of NIH growth; (iii) output module: the model's performance is evaluated by comparing the simulated vessel geometry to clinical scans. Detailed explanations of each module are provided in the following subsections.

2.1. Patient dataset

We considered one PAD patient who underwent femoropopliteal bypass surgery using an autogenous vein graft. CT scans were available at baseline and at 10-month follow-up (10M FU). DUS images were collected at the same time point ("Matching") as the baseline CT scan acquisition, and at 12-, 6-months before (12M prior, 6M prior, respectively) and 2-months after (2M FU). Given the availability of a 10M FU CT scan, we conducted predictive computations of long-term NIH growth. The deidentified data were obtained from VA Connecticut Healthcare Systems (West Haven, CT, USA) and the study received ethical approval from the West Haven VA Connecticut Healthcare Systems (approval number AD0009).

2.2. Vessel reconstruction and patient-specific CFD module

The femoropopliteal vessel was segmented and 3D reconstructed using a previously validated semi-automatic algorithm (Colombo et al., 2020) implemented in MATLAB (MathWorks, Natick, MA, USA). The bypass reconstruction was carried out until reaching areas with suboptimal contrast agent visibility.

The fluid domain was discretised using a combination of tetrahedral elements with 5 layers of prismatic elements near the wall, employing ICEM CFD (Ansys Inc., Canonsburg, PA, USA). Meshing parameters were set according to a previous mesh independence study (Colombo et al., 2020).

Transient CFD simulations were performed for each available DUS. The Navier-Stokes and continuity equations were solved using the finite volume-based code Fluent (Ansys Inc.). The numerical schemes employed are detailed in (Colombo et al., 2020). The flow was assumed to be laminar (Colombo et al., 2020). The blood density was considered constant ($\rho = 1060$ kg/m^3), and its non-Newtonian behaviour was modelled using the Carreau model (Colombo et al., 2020). For BCs, the velocity waveform acquired at the common femoral artery level was manually extracted from the DUS spectrum and imposed at the inlet, after the sequence of peak velocities was elaborated in MATLAB by applying the algorithm of (Ponzini et al., 2006), as detailed in (Colombo et al., 2020). Due to the absence of patient-specific information, a literature-derived flow split of 0.33:0.67 was applied at the profunda femoral and bypass outlets, respectively (Klein et al., 2003). The vessel wall was assumed to be rigid, with no-slip conditions.

TAWSS, defined as the average magnitude of the wall shear stress vector over the cardiac cycle (Eq. (1), Supplementary Material), was evaluated along the bypass length for each inlet BC. This served as input to the "Remodelling module" described next.

2.3. Remodelling module

This module, implemented in MATLAB, allowed for the calculation of media and intimal volume growth, leading to the gradual loss of vein graft patency (Fig. 1). SMC proliferation in the vessel's intima layer was considered the most critical response from vascular tissue after injury caused by vein graft implantation (Boyle et al., 2010; Model & Dardik, 2012). Here, the subscripts *i* and *m* refer to the intima and media layers,

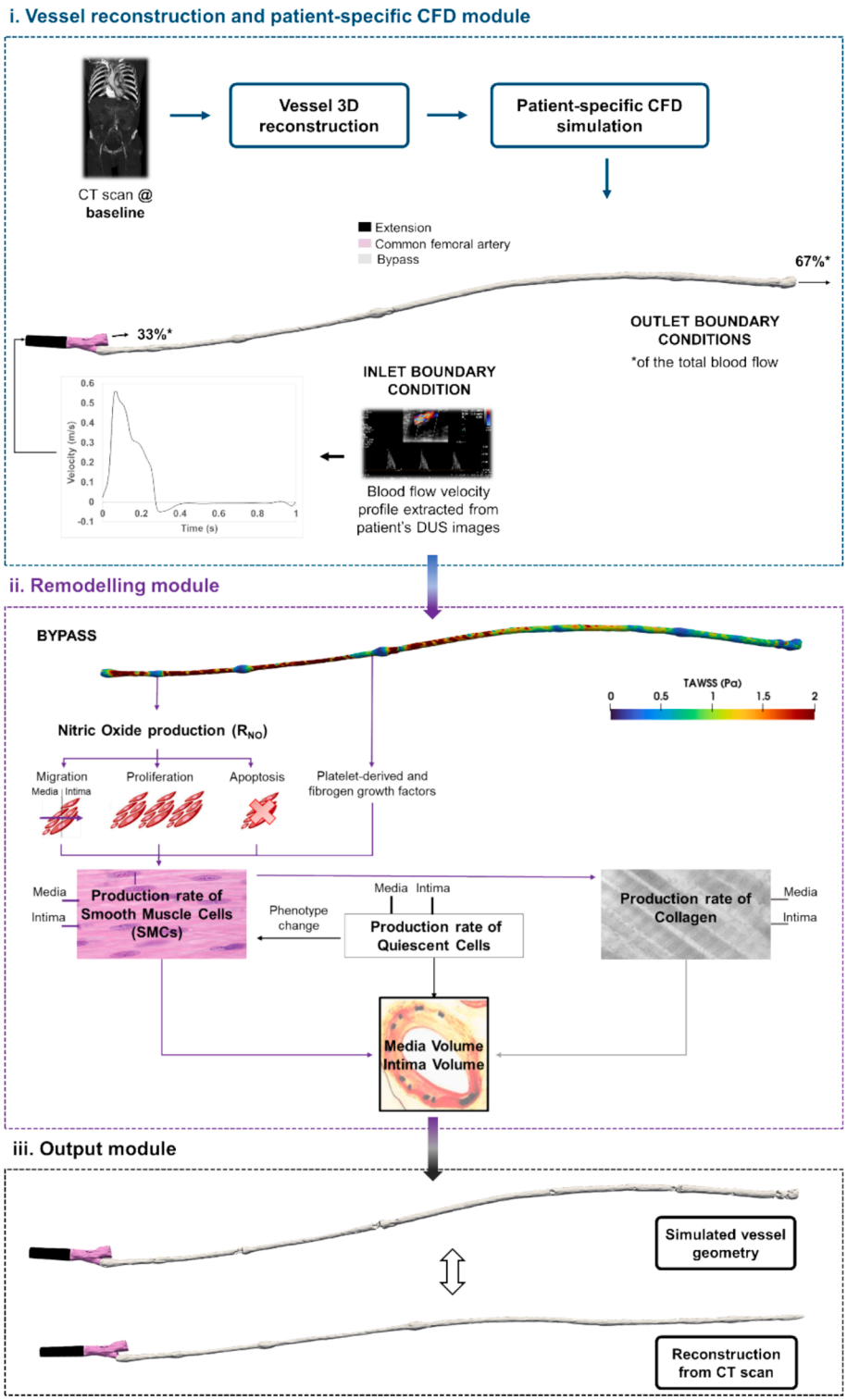

Fig. 1. Computational workflow applied to simulate NIH growth.

respectively. In this study, these layers were not individually modelled. The focus was on the cumulative effect/impact of patient-specific hemodynamics and biochemical processes on NIH growth, which leads to vessel geometry modification over time. Table 1 lists the constant parameters used in the model with their respective values and literature references.

The final media (V_m) and intimal (V_i) volumes were assumed to be dependent on the production rate of quiescent cells (Q), collagen (C) and SMCs (S) (Eqs. (1) and (2), with ρ_s and ρ_c being cell and collagen density (Table 1), respectively.

$$V_i = (S_i + Q_i) \times \rho_s^{-1} + C_i \times \rho_c^{-1} \quad (1)$$

$$V_m = (S_m + Q_m) \times \rho_s^{-1} + C_m \times \rho_c^{-1} \quad (2)$$

The rate of quiescent cell production was modelled through logistic growth equations (Eqs. (3) and (4), Table 1), following a previously used cell modelling approach for tumour growth (Kozusko & Bourdeau, 2007;

Table 1
Constant parameters used in the "Remodelling module" with the respective literature references.

Parameter	Value	Reference
ρ_s = cell density	2.18×10^{14} cells/m^3	(Schwartz et al., 1992)
ρ_c = collagen density	2×10^3 g/m^3	(Humphrey & Epstein, 2002)
β = turnover of quiescent cells	5×10^{-4} day^{-1}	(Davies & Hagen, 1994)
λ = collagen production rate	2.16×10^{-13} g/(day × cell)	(Cilla et al., 2014)
χ = collagen degradation rate	0.033 day^{-1}	(Cilla et al., 2014)
γ = rate at which quiescent cells differentiate into SMCs	10^{-4} day^{-1}	(Davies & Hagen, 1994)
ϕ = coefficient of production due to growth factors	10^{-6} cells/(ng × day)	(Davies & Hagen, 1994)

Marušic et al., 1994). The maximum number of cells $Q_{i,\max}$ and $Q_{m,\max}$ was calculated based on the maximum volume available in the intima and media layer, respectively. Ω_i and Ω_m represent the intima and media domains, respectively.

$$\frac{dQ_i}{dt} = \beta \times Q_i \times \left(1 - \frac{Q_i}{Q_{i,max}}\right) in\Omega_i \tag{3}$$

$$\frac{dQ_m}{dt} = \beta \times Q_m \times \left(1 - \frac{Q_m}{Q_{m,max}}\right) in\Omega_m \tag{4}$$

The rate of collagen production was estimated following the approach proposed by (Cilla et al., 2014) (Eqs. (5) and (6), with λ and χ being the collagen production and degradation rate (Table 1), respectively.

$$\frac{dC_i}{dt} = S_i \times \lambda - C_i \times \chi in\Omega_i \tag{5}$$

$$\frac{dC_m}{dt} = S_m \times \lambda - C_m \times \chi in\Omega_m \tag{6}$$

The rate of production of SMCs was modelled as dependent on cell phenotype change (Zain et al., 2022) from quiescent cells, migration to the intima layer, production/apoptosis of cells and presence of platelet-derived (PDGF) and fibroblast (FGF-2) growth factors (Eqs. (7) and (8), Table 1).

$$\frac{dS_i}{dt} = \gamma \times Q_i + ((p_i - a_i) \times S_i + m \times S_m) + \phi \times (G_P + G_F) in\Omega_i \tag{7}$$

$$\frac{dS_m}{dt} = \gamma \times Q_m + (p_m - a_m - m) \times S_m in\Omega_m \tag{8}$$

The equations regarding PDGF (G_p) and FGF-2 (G_F) presence (Eqs. (2) and (3), Supplementary Material) followed the general form given by (Budu-Grajdeanu et al., 2008). The growth rates for PDGF and FGF-2 (Table 1, Supplementary Material) were estimated from the literature (Palumbo et al., 2002; Reisig & Clyne, 2010), whereas the degradation coefficients (Table 1, Supplementary Material), dependent on TAWSS, followed the work of (Cilla et al., 2014). The coefficients regarding migration, production and apoptosis of SMCs in the intima layer (m, p_i and a_i) (Table 1, Supplementary Material) were assumed to vary linearly with the NO production rate (R_{NO}) (Marks et al., 1995; Nishio et al., 1996). Specifically, a higher production of NO, linked to high values of TAWSS, inhibited NIH formation (Ahanchi et al., 2007; Pearce et al., 2008). Constant values for the migration, production and apoptosis coefficients (m_0, p_m and a_m) were used for the media layer (Table 1, Supplementary Material).

2.3.1. Relationship between R_{NO} and TAWSS

The relationship between NO production and TAWSS is typically obtained from experimental data assuming different fittings (Andrews et al., 2010; Chen et al., 2011; Fadel et al., 2009; Plata et al., 2010). In (Donadoni et al., 2017), a linear model (Andrews et al., 2010) was chosen (Eq. (9)) since it produced results closer to the experimental values for TAWSS lower than 0.5 Pa, below which NIH is more likely to develop (Meirson et al., 2015). However, evidence in the literature (Andrews et al., 2010) suggests that a hyperbolic relationship (Eq. (10)) best describes the experimental data, followed by a sigmoidal one (Eq. (11)), which has nevertheless been reported to produce unphysiological trends at high TAWSS values (Andrews et al., 2010).

$$R_{NO} = 1.74(nM/s) + 75.2(nM/s/Pa) \times TAWSS(Pa) \tag{9}$$

$$R_{NO} = 2.13(nM/s) + 457.5(nM/s) \times \frac{TAWSS(Pa)}{(TAWSS(Pa) + 3.5(Pa))} \tag{10}$$

$$R_{NO} = \frac{129.5(nM/s)}{(1 + 115 \times e^{-5(Pa^{-1}) \times TAWSS(Pa)})} \tag{11}$$

All three fittings were tested on the available patient data to identify the TAWSS-NO relationship that best predicts NIH growth within the graft. For this purpose, the "Matching" DUS was applied as inlet BC to compute TAWSS.

2.3.2. Remodelling quantification

Once the intimal and media volumes were computed at each node for the simulated follow-up, the displacement (in mm) of each node in the 3D space was derived by dividing the volume by the corresponding cell surface area. The total remodelling, given by the sum of intimal and media volumes, was also constrained such that it could not increase if it had reached the total available volume defined by the bypass geometry.

3D maps of displacement were re-organised into two-dimensional (2D) maps by unfolding the bypass geometry (Colombo et al., 2021a) using the open-source software VMTK (Orobix, Bergamo, Italy). The 2D maps were discretised in the axial and circumferential direction (cells of 1 mm and 1°, respectively) and then circumferentially averaged to obtain one-dimensional (1D) displacements with an axial resolution of 1 mm (Colombo et al., 2021a) (Fig. 2). The 1D displacements were then subtracted at the corresponding locations from the radius of the baseline vein graft. This allowed us to compare the predicted bypass geometry with the reconstructed geometry at 10M (based on CT scans).

2.4. Output module

This module compared the predicted/computed bypass geometry with the actual vein graft geometry reconstructed from the follow-up (10M FU). The performance of the model was based on co-localising the areas subjected to restenosis between the simulated and the reconstructed geometry.

3. Results

3.1. Predicting long-term restenosis using different $TAWSS - R_{NO}$ relationships

The *predicted* vascular remodelling of the available patient was compared against the reconstructed CT images at 10M FU. Fig. 3 shows the vein graft diameter at baseline and at 10M FU. Locations presenting critical restenosis, defined by a diameter reduction greater than 50%, are indicated in both the simulation results and the CT scan-reconstructed geometry, using red and blue symbols, respectively. All three TAWSS-R_{NO} models predicted critical restenosis in the distal part of the bypass, where total occlusion occurred. However, the linear and sigmoidal models generally overestimated the remodelling along the whole graft (Fig. 3). The hyperbolic model appeared to better capture the graft diameter evolution. However, it predicted severe restenosis in

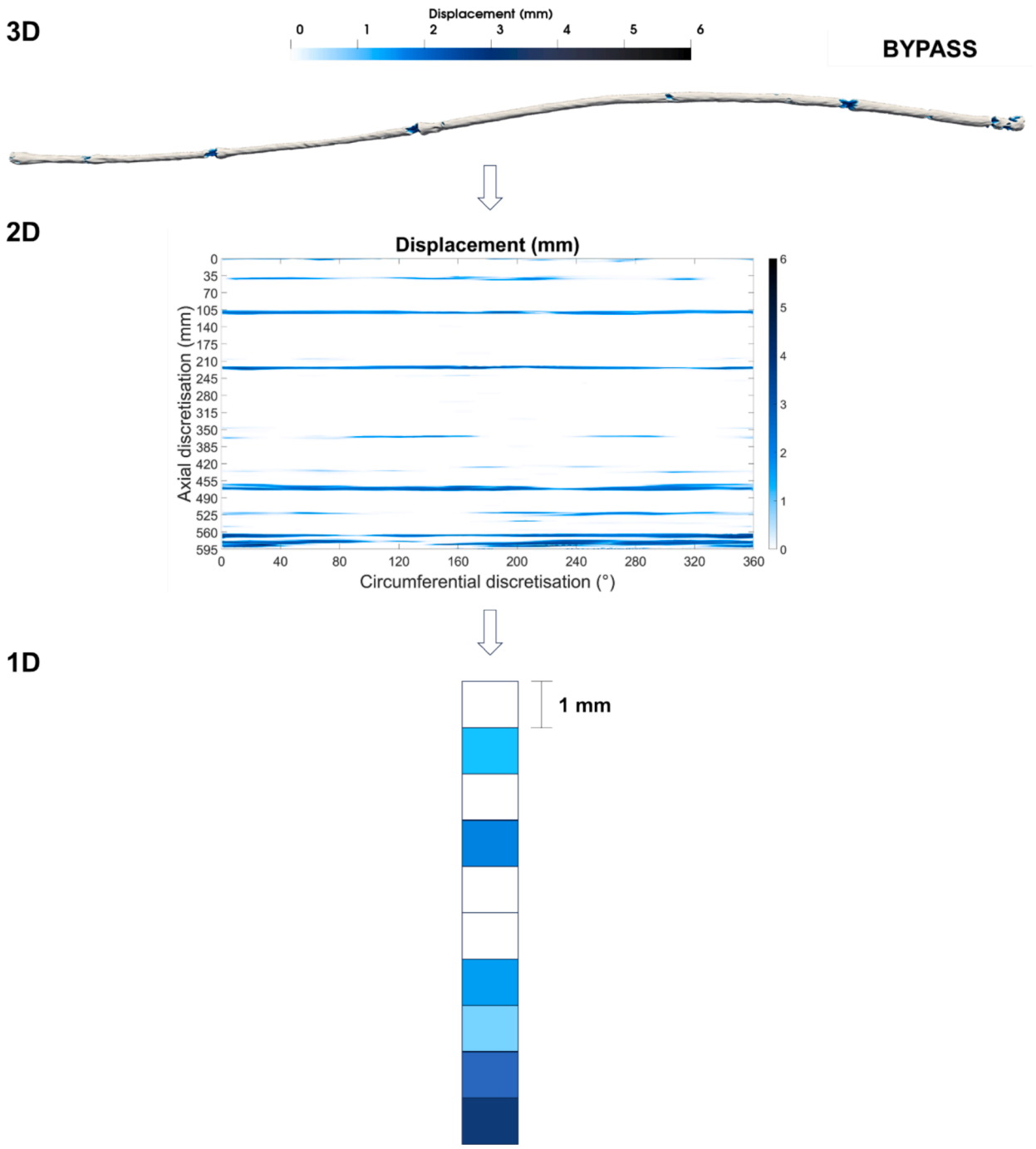

Fig. 2. From 3D to 1D maps of displacement. 3D maps of displacement were re-organised into 2D maps for every tested TAWSS-NO relationship. The 2D maps were discretised in the axial and circumferential direction (cells of 1 mm and 1°, respectively). 1D displacement with an axial resolution of 1 mm was obtained by circumferentially averaging the 2D maps.

certain locations that did not appear prone to NIH growth (Fig. 3). These regions, identified as critical even using linear and sigmoidal models, coincided with the locations of the vein graft valves, as observed (Fig. 3). Notably, these valves are rarely reported as critical areas of interest (Vesti et al., 2001). Therefore, upon clinical interpretation, these regions could be excluded from our analysis.

Overall, the hyperbolic model emerged as the most suitable, accurately predicting restenosis $\geq 50\%$ in the distal part of the bypass at 10M follow-up, *whilst simultaneously* minimising the number of 'false' regions undergoing severe restenosis (Fig. 3). Thus, the hyperbolic TAWSS-R_{NO} relationship was selected for the sensitivity analyses to inflow BCs described in the following sections.

3.2. Sensitivity of predictions to inlet BCs

This element of the computational pipeline is critical, given the strong evidence in the literature that highlights luminal regions exposed to low/oscillatory wall shear stress as fundamental building blocks in understanding vessel response to the local environment and the resulting vascular remodelling and NIH growth. In our case, we had different DUS measurements acquired at different timepoints (either before or after the baseline CT scan acquisition). Thus, we were able to evaluate the sensitivity of the model's predictions to TAWSS values calculated using these different waveforms. This allowed us to determine whether the regions undergoing total occlusion at 10M could be predicted even

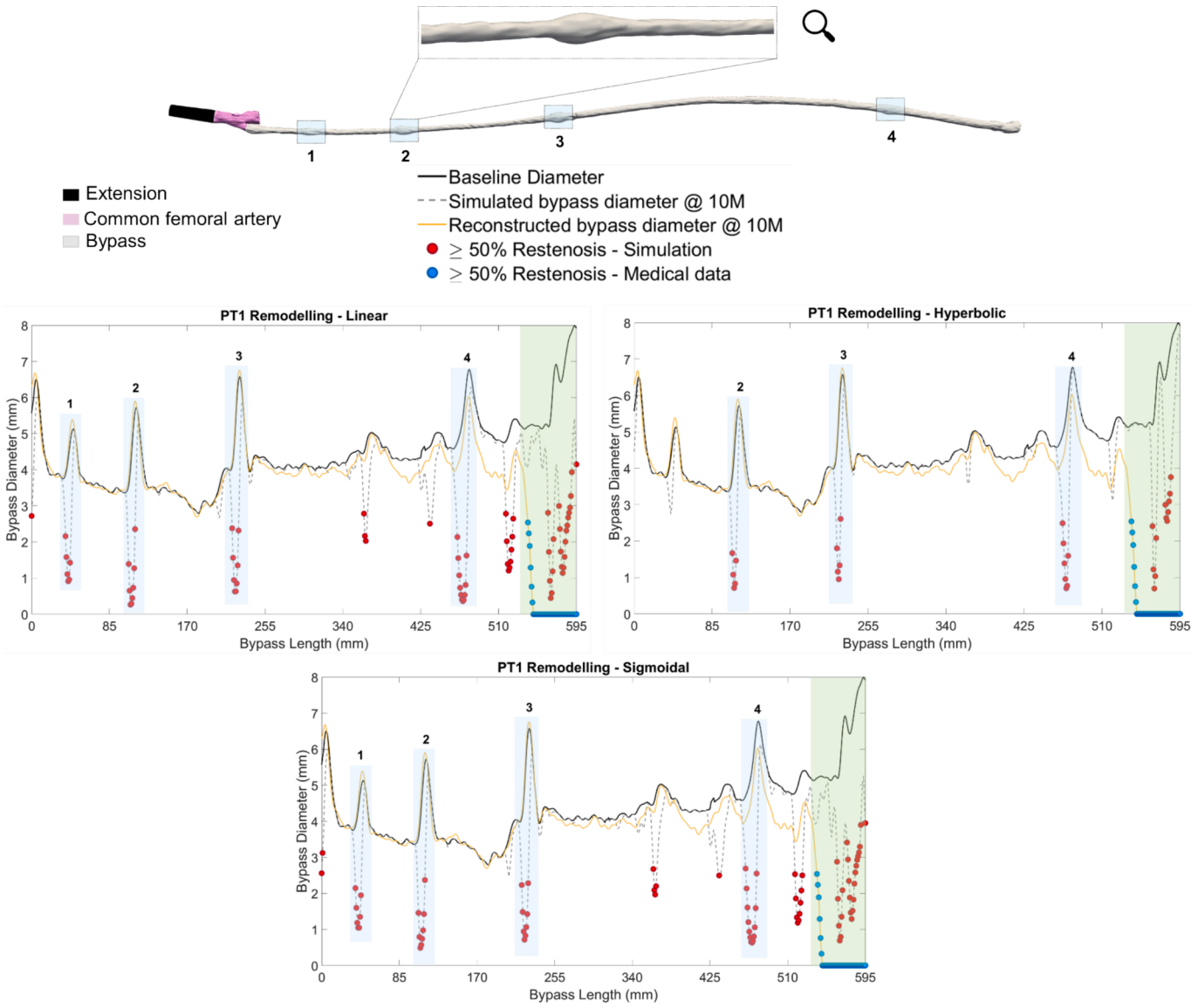

Fig. 3. Baseline femoropopliteal geometry of the available patient (PT1) and corresponding baseline, simulated and reconstructed from medical images bypass diameter, using linear, hyperbolic and sigmoidal TAWSS-R_{NO} relationships. Locations presenting critical restenosis (diameter reduction $\geq$ 50 %) are indicated in both the simulation results and the CT scan-reconstructed geometry, using red and blue symbols, respectively. All three TAWSS-R_{NO} models predicted critical restenosis in the distal part of the bypass, where total occlusion occurred (green shaded regions). Light blue shaded regions indicate vein graft valves, which rarely undergo restenosis (Vesti et al., 2001). The hyperbolic model was the one predicting best the diameter evolution, minimising the number of 'false' regions undergoing severe restenosis compared to the other models.

with inflow conditions that did not reflect the exact patient hemodynamic state at baseline.

Fig. 4 shows the different velocity waveforms extracted from the patient's DUS images used as inlet BCs and corresponding TAWSS distributions. Waveform characteristics (i.e., waveform shape, peak systolic velocity, systolic acceleration time and cardiac cycle period) are summarised in Table 2, whereas Table 3 shows the median, maximum and minimum values of the respective TAWSS distributions. The Matching, 6M prior and 2M FU DUS-derived velocity waveforms were biphasic, whereas the 12M prior was triphasic. The 12M prior, Matching, and 2M FU waveforms had comparable systolic acceleration time, although the latter had a lower peak systolic velocity compared to the former ones. Critically, a non-parametric Wilcoxon test revealed that all estimated TAWSS distributions were statistically significantly different (p-value < 0.01) from the reference "Matching" case (Fig. 4.b).

Fig. 5 compares the baseline, the reconstruction-derived and the simulated vein graft diameters, for different applied inlet BCs. In the distal portion of the bypass, restenosis of $\geq$ 50% was predicted for all inlet BCs, although statistically significantly different TAWSS values were obtained compared to the "Matching" case. However, using the 2M FU DUS waveform as inlet BC produced remodelling predictions closer to those obtained with the "Matching" BC. The reason why is that the respective TAWSS distributions were comparable in terms of median, minimum and maximum values (Table 3), and leading to a similar NO production and vascular remodelling. Conversely, TAWSS distributions associated with 6M and 12M prior DUS predicted less remodelling, since their TAWSS distributions shifted to higher values compared to the reference one (Fig. 4.b, Table 3). Overall, remodelling predictions were closer to the reference ("Matching") case when the shapes of the inflow waveform were similar and their systolic acceleration times comparable (Ninno et al., 2024).

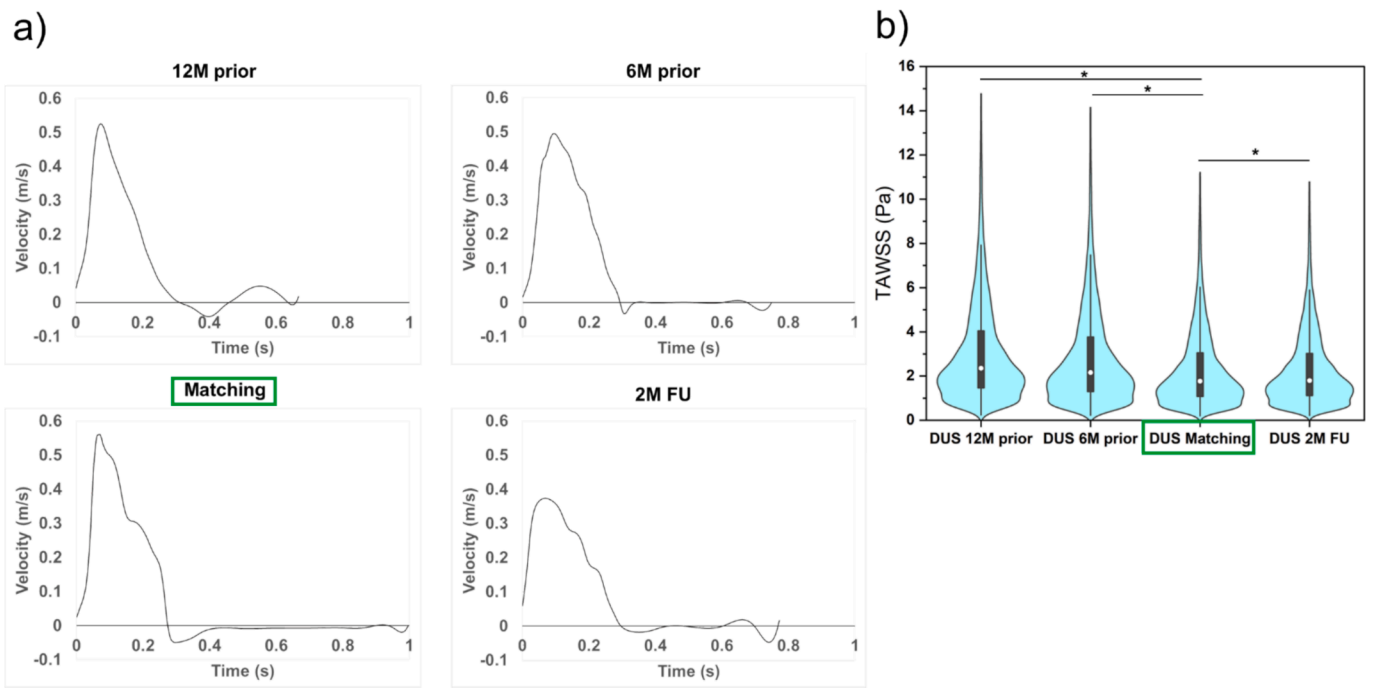

Fig. 4. (a) Extracted waveforms from DUS images for the available patient, acquired at the same time ("Matching") or before ("prior")/following-up ("FU") the CT scan acquisition; (b) Corresponding TAWSS distributions obtained by applying the waveforms as inlet BCs. Pairwise comparisons with respect to the reference distribution using the non-parametric Wilcoxon test showed significant differences (*p-value < 0.01). The reference waveform and TAWSS distribution ("Matching") are highlighted by a rectangle.

Table 2
DUS-derived waveforms' characteristics of the available patient regarding acquisition time with respect to the CT scan, waveform shape, peak systolic velocity, systolic acceleration time and cardiac cycle period.

Acquisition time	Waveform shape	Peak Systolic Velocity (m/s)	Systolic acceleration time (s)	Cardiac cycle period (s)
Matching	Biphasic	0.560	0.070	1.007
12M prior	Triphasic	0.525	0.074	0.674
6M prior	Biphasic	0.494	0.091	0.757
2M FU	Biphasic	0.374	0.070	0.781

Table 3
Median, maximum and minimum values of the TAWSS distributions obtained by applying as inlet BCs the corresponding DUS for the available patient.

Corresponding DUS	Median (Pa)	Maximum (Pa)	Minimum (Pa)
Matching	1.77	19.38	0.19
12M prior	2.36	26.23	0.24
6M prior	2.17	25.38	0.22
2M FU	1.80	21.32	0.21

4. Discussion

The present study involved the development of a new and efficient computational pipeline for NIH prediction in lower-limb vein grafts. This pipeline analyses the entire vein graft remodelling rather than focusing on selected locations only and uses routinely available medical imaging for PAD. Our analysis emphasises the importance of coherent data collection and the use of consistent datasets to accurately capture the patient's true hemodynamic state, given the well-established strong link between hemodynamics and vascular remodelling.

The rationale behind this work lies in the extensive research on multiscale *in silico* models of vascular adaptation (Corti et al., 2021), which aim to capture the complex nature of vascular pathologies and depict the driving mechanisms of response to interventions. Currently, these models come with certain limitations, including high computational costs, reliance on fragmented medical datasets and unavailability of key information required to inform the models, such as data at the molecular level (Corti et al., 2022b). Therefore, refining and testing a parsimonious continuum model that relies solely on *available* medical data is a valid option in the landscape prediction models of vein graft remodelling.

The main findings of the study can be summarised as follows: (i) a hyperbolic TAWSS-R_{NO} relationship provides the best prediction in terms of lumen diameter evolution and identifying graft locations undergoing $\geq$ 50% restenosis at 10M follow-up. This is in line with the work by (Andrews et al., 2010), in which the hyperbolic fitting showed the closest match to the experimental data; (ii) a DUS-derived inlet velocity profile that is not representative of the actual patient-specific hemodynamic condition potentially leads to wrong predictions, since statistically significantly different TAWSS distributions with respect to the reference case are obtained. Nevertheless, NIH predictions become more accurate when an inlet waveform having the same shape and comparable systolic acceleration time to the one "Matching" in time the CT scan acquisition is applied. This information can be retrieved from the DUS examination report, conducted when acquiring a CT scan, and always stored. The fact that the lack of a "Matching" DUS can be somewhat compensated by choosing another patient-specific waveform with similar characteristics (independently of the performed interventions in between) is in agreement with our previous findings regarding the impact of inflow conditions on CFD results (Ninno et al., 2024).

Several considerations have to be taken into account while interpreting the findings of this study.

The choice of the best TAWSS-R_{NO} relationship for predicting long-term NIH growth was based on data from a single patient due to the limited availability of clinical data. Future studies, involving larger datasets, will help further test and validate the model. However, it is

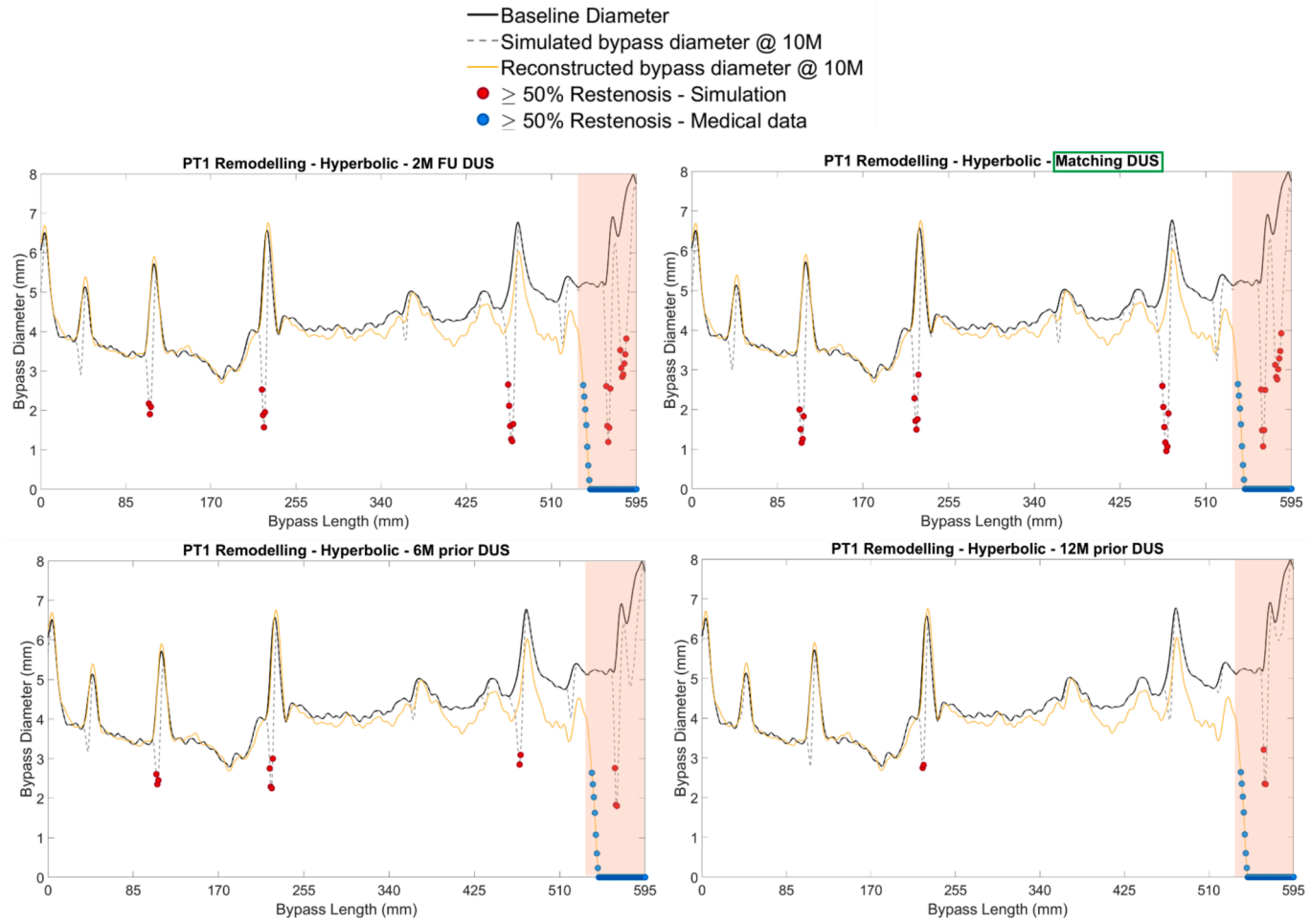

Fig. 5. Baseline, reconstruction-derived and the simulated vein graft diameters, obtained with the different applied inlet BCs on the available patient (PT1). Restenosis higher than 50 % was predicted for all inlet BCs tested in the distal part of the bypass (light orange shaded regions). The 2M FU DUS inlet BC led to closer results to the reference one ("Matching DUS", highlighted by a rectangle), due to a similarity in the respective TAWSS distributions (Fig. 4b).

important to note that the primary focus of the current study is on the computational pipeline, which enables the prediction of NIH growth along the entire vein graft.

TAWSS values were not updated over the simulated time period due to the absence of DUS images between the baseline and follow-up CT scans. Nevertheless, our results are promising, highlighting the potential of this proof-of-concept model.

The model does not account for the processes linked to the inflammatory response following the intervention, despite its crucial role in accelerating the remodelling within the first days to weeks (de Vries & Quax, 2018; Garbey & Berceli, 2013; Jiang et al., 2009). This can lead to a reduction in the lumen area within the first month of follow-up, after which the inflammatory state resolves (Corti et al., 2022a). Given that the effect of inflammation is pronounced only during the first few weeks after intervention, it is also reasonable to believe that the conclusions obtained for the long-term follow-up would remain unchanged, even if inflammation had been included in the model. Any additional remodelling would reinforce the already predicted significant changes in the bypass diameter. However, information regarding the inflammatory response is not routinely collected in clinical practice and might be crucial to predict vascular remodelling in shorter timescales.

The key parameters of the model (Table 1 in the Manuscript and Table 1 in Supplementary Material) are not patient-specific, but literature-derived. Although an option for calibration could be based on minimising the difference between the simulated lumen area and the patient (real) lumen area observed at follow-up (Corti et al., 2022b; Corti et al., 2023) which could potentially improve model's results, it is important to note that *a priori* predictions cannot be made in the absence of follow-up data. It is also likely that many models would need to be run, and numerous datasets collected, to effectively pivot these types of analyses toward predictions for new patients, given patient variability in a normal population as well as the non-negligible influence of co-morbidities, aging and lifestyle.

The proposed model demonstrates that combining mechanistic biochemical models with patient-specific hemodynamics shows promise in predicting NIH progression in PAD patients. The computational pipeline is easily expandable, since the equations that calculate neointimal growth are all ODEs and implemented in MATLAB. Furthermore, the computational cost of the model is modest; the "Remodelling module" runs in MATLAB in minutes, while the hemodynamic computations take around 36 h on a Cluster (Intel® Xeon® Gold 5118 at 2.3 GHz using 10 processors) for transient simulations of meshes 3,000,000 elements. The computational/running time could potentially be reduced by performing steady-state simulations and assessing the impact on predictions, or by applying reduced-order techniques for fast CFD analyses (Buoso et al., 2019; Chatpattanasiri et al., 2023). These combined with future work on the effects of stent implantation and injury score (Boyle et al., 2010), could extend the model applicability to stented femoral arteries, paving the way towards clinical translation of such predictive tools.

5. Conclusions

In this study, we presented a new and efficient computational pipeline for simulating NIH growth in lower-limb vein grafts, based on the previous work by (Donadoni et al., 2017), and we tested its suitability for predicting long-term remodelling using available clinical data. As a proof-of-concept, various relationships between TAWSS and NO production derived from published experimental data were tested, and the robustness of the model in dealing with non-standardised collected data in PAD was assessed on one patient. This entailed patient-specific hemodynamic analyses using inlet DUS-derived waveforms not acquired at the same time as the baseline CT scan used for vessel geometry reconstruction. The results revealed that a hyperbolic TAWSS-R_{NO} relationship predicts well the long-term vein graft response. The model is robust to inlet BCs, as long as the applied waveform has the same shape and comparable systolic acceleration time to that recorded at the time of the CT acquisition. The model is also easily expandible and provides a relatively efficient (in terms of computational effort) foundational platform to perform long-term analyses for vein-graft remodelling. This suggests that the multiscale model has the potential to predict NIH progression in lower-limb vein grafts and inform clinicians on disease progression by identifying graft locations more prone to restenosis, while only requiring readily available clinical data. It is imperative to collect coherent and longitudinal data to validate the multiscale model and conduct further research to strengthen the findings of the present study.

CRediT authorship contribution statement

Federica Ninno: Writing – review & editing, Writing – original draft, Visualization, Methodology, Formal analysis, Data curation, Conceptualization. **Claudio Chiastra:** Writing – review & editing, Writing – original draft, Supervision. **Francesca Donadoni:** Methodology. **Alan Dardik:** Writing – original draft, Data curation. **David Strosberg:** Writing – original draft, Data curation. **Edouard Aboian:** Writing – original draft, Data curation. **Janice Tsui:** Writing – original draft, Supervision. **Stavroula Balabani:** Writing – review & editing, Writing – original draft, Supervision, Data curation. **Vanessa Díaz-Zuccarini:** Writing – review & editing, Writing – original draft, Supervision, Methodology, Data curation, Conceptualization.

Funding

This work was funded by the University College London EPSRC Centre for Doctoral Training i4health [EP/S021930/1] and the Wellcome/EPSRC Centre for Interventional and Surgical Sciences (WEISS) [203145Z/16/Z]; and supported by researcher (JT) at the National Institute for Health Research University College London Hospitals Biomedical Research Centre. We also acknowledge the BBRC International Institutional Awards University College London (IIA Tranche 1 UCL) and the use of facilities and resources at the VA Connecticut Healthcare System, West Haven, CT, USA.

Declaration of competing interest

The authors declare that they have no known competing financial interests or personal relationships that could have appeared to influence the work reported in this paper.

Appendix A. Supplementary material

Supplementary data to this article can be found online at https://doi.org/10.1016/j.jbiomech.2024.112428.

References

Ahanchi, S.S., Tsihlis, N.D., Kibbe, M.R., 2007. The role of nitric oxide in the pathophysiology of intimal hyperplasia. *J. Vasc. Surg.* 45 (6 SUPPL.). https://doi.org/10.1016/j.jvs.2007.02.027.

Andrews, A.M., Jaron, D., Buerk, D.G., Kirby, P.L., Barbee, K.A., 2010. Direct, real-time measurement of shear stress-induced nitric oxide produced from endothelial cells in vitro. *Nitric Oxide – Biol. Chem.* 23 (4). https://doi.org/10.1016/j.niox.2010.08.003.

Boyle, C.J., Lennon, A.B., Early, M., Kelly, D.J., Lally, C., Prendergast, P.J., 2010. Computational simulation methodologies for mechanobiological modelling: A cell-centred approach to neointima development in stents. *Philos. Trans. R. Soc. A Math. Phys. Eng. Sci.* 368 (1921). https://doi.org/10.1098/rsta.2010.0071.

Budu-Grajdeanu, P., Schugart, R.C., Friedman, A., Valentine, C., Agarwal, A.K., Rovin, B. H., 2008. A mathematical model of venous neointimal hyperplasia formation. *Theor. Biol. Med. Model.* 5. https://doi.org/10.1186/1742-4682-5-2.

Buoso, S., Manzoni, A., Alkadhi, H., Plass, A., Quarteroni, A., Kurtcuoglu, V., 2019. Reduced-order modeling of blood flow for noninvasive functional evaluation of coronary artery disease. *Biomech. Model. Mechanobiol.* 18 (6). https://doi.org/10.1007/s10237-019-01182-w.

Chaabane, C., Otsuka, F., Virmani, R., Bochaton-Piallat, M. L. (2013). Biological responses in stented arteries. In: *Cardiovascular Research,* vol. 99, Issue 2. 10.1093/cvr/cvt115.

Chatpattanasiri, C., Franzetti, G., Bonfanti, M., Diaz-Zuccarini, V., Balabani, S., 2023. Towards reduced order models via robust proper orthogonal decomposition to capture personalised aortic haemodynamics. *J. Biomech.* 158. https://doi.org/10.1016/j.jbiomech.2023.111759.

Chen, X., Buerk, D.G., Barbee, K.A., Kirby, P., Jaron, D., 2011. 3D network model of NO transport in tissue. *Med. Biol. Eng. Compu.* 49 (6). https://doi.org/10.1007/s11517-011-0758-7.

Chiastra, C., Dubini, G., Migliavacca, F., 2021a. Hemodynamic perturbations due to the presence of stents. In *Biomechanics of Coronary Atherosclerotic Plaque: From Model to Patient*. 10.1016/B978-0-12-817195-0.00011-1.

Chiastra, C., Dubini, G., Migliavacca, F., 2021b. Modeling the stent deployment in coronary arteries and coronary bifurcations. In: *Biomechanics of Coronary Atherosclerotic Plaque: From Model to Patient*. 10.1016/B978-0-12-817195-0.00026-3.

Cilla, M., Peña, E., Martínez, M.A., 2014. Mathematical modelling of atheroma plaque formation and development in coronary arteries. *J. R. Soc. Interface* 11 (90). https://doi.org/10.1098/rsif.2013.0866.

Colombo, M., Bologna, M., Garbey, M., Berceli, S., He, Y., Rodriguez Matas, J.F., Migliavacca, F., Chiastra, C., 2020. Computing patient-specific hemodynamics in stented femoral artery models obtained from computed tomography using a validated 3D reconstruction method. *Med. Eng. Phys.* https://doi.org/10.1016/j.medengphy.2019.10.005.

Colombo, M., He, Y., Corti, A., Gallo, D., Casarin, S., Rozowsky, J.M., Migliavacca, F., Berceli, S., Chiastra, C., 2021a. Baseline local hemodynamics as predictor of lumen remodeling at 1-year follow-up in stented superficial femoral arteries. *Sci. Rep.* 11 (1). https://doi.org/10.1038/s41598-020-80681-8.

Colombo, M., He, Y., Corti, A., Gallo, D., Ninno, F., Casarin, S., Rozowsky, J.M., Migliavacca, F., Berceli, S., Chiastra, C., 2021b. In-stent restenosis progression in human superficial femoral arteries: dynamics of lumen remodeling and impact of local hemodynamics. *Ann. Biomed. Eng.* 49 (9). https://doi.org/10.1007/s10439-021-02776-1.

Corti, A., Colombo, M., Migliavacca, F., Berceli, S.A., Casarin, S., Rodriguez Matas, J.F., Chiastra, C., 2022a. Multiscale agent-based modeling of restenosis after percutaneous transluminal angioplasty: Effects of tissue damage and hemodynamics on cellular activity. *Comput. Biol. Med.* 147. https://doi.org/10.1016/j.compbiomed.2022.105753.

Corti, A., Colombo, M., Rozowsky, J.M., Casarin, S., He, Y., Carbonaro, D., Migliavacca, F., Rodriguez Matas, J.F., Berceli, S.A., Chiastra, C., 2022b. A predictive multiscale model of in-stent restenosis in femoral arteries: linking haemodynamics and gene expression with an agent-based model of cellular dynamics. *J. R. Soc. Interface* 19 (188).

Corti, A., Colombo, M., Migliavacca, F., Rodriguez Matas, J. F., Casarin, S., Chiastra, C., 2021. Multiscale Computational Modeling of Vascular Adaptation: A Systems Biology Approach Using Agent-Based Models. In: *Frontiers in Bioengineering and Biotechnology* (Vol. 9). 10.3389/fbioe.2021.744560.

Corti, A., Migliavacca, F., Berceli, S.A., Chiastra, C., 2023. Predicting 1-year in-stent restenosis in superficial femoral arteries through multiscale computational modelling. *J. R. Soc. Interface* 20 (201). https://doi.org/10.1098/rsif.2022.0876.

Criqui, M. H., Matsushita, K., Aboyans, V., Hess, C. N., Hicks, C. W., Kwan, T. W., McDermott, M. M., Misra, S., Ujueta, F., 2021. Lower Extremity Peripheral Artery Disease: Contemporary Epidemiology, Management Gaps, and Future Directions: A Scientific Statement from the American Heart Association. In *Circulation* (Vol. 144, Issue 9). 10.1161/CIR.0000000000001005.

Davies, M. G., Hagen, P. -O., 1994. Pathobiology of intimal hyperplasia. In *British Journal of Surgery* (Vol. 81, Issue 9). 10.1002/bjs.1800810904.

de Vries, M. R., Quax, P. H. A., 2018. Inflammation in Vein Graft Disease. In: *Frontiers in Cardiovascular Medicine* (Vol. 5). 10.3389/fcvm.2018.00003.

Donadoni, F., Pichardo-Almarza, C., Bartlett, M., Dardik, A., Homer-Vanniasinkam, S., Díaz-Zuccarini, V., 2017. Patient-specific, multi-scale modeling of neointimal hyperplasia in vein grafts. *Front. Physiol.* 8 (APR). https://doi.org/10.3389/fphys.2017.00226.

Fadel, A.A., Barbee, K.A., Jaron, D., 2009. A computational model of nitric oxide production and transport in a parallel plate flow chamber. *Ann. Biomed. Eng.* 37 (5). https://doi.org/10.1007/s10439-009-9658-5.

Garbey, M., Berceli, S.A., 2013. A dynamical system that describes vein graft adaptation and failure. *J. Theor. Biol.* 336. https://doi.org/10.1016/j.jtbi.2013.07.006.
Gosak, M., Markovič, R., Dolenšek, J., Slak Rupnik, M., Marhl, M., Stožer, A., Perc, M., 2018. Network science of biological systems at different scales: A review. *Phys. Life Rev.* 24. https://doi.org/10.1016/j.plrev.2017.11.003.
Humphrey, J., Epstein, M., 2002. Cardiovascular solid mechanics: cells, tissues, and organs. *Appl. Mech. Rev.* 55 (5). https://doi.org/10.1115/1.1497492.
Hwang, M., Garbey, M., Berceli, S. A., Tran-Son-Tay, R., 2009. Rule-based simulation of multi-cellular biological systems-a review of modeling techniques. In *Cellular and Molecular Bioengineering* (Vol. 2, Issue 3). 10.1007/s12195-009-0078-2.
Jiang, Z., Yu, P., Tao, M., Ifantides, C., Ozaki, C.K., Berceli, S.A., 2009. Interplay of CCR2 signaling and local shear force determines vein graft neointimal hyperplasia in vivo. *FEBS Lett.* 583 (21). https://doi.org/10.1016/j.febslet.2009.10.015.
Klein, W.M., Bartels, L.W., Bax, L., Van der Graaf, Y., Mali, W.P.T.M., 2003. Magnetic resonance imaging measurement of blood volume flow in peripheral arteries in healthy subjects. *J. Vasc. Surg.* https://doi.org/10.1016/S0741-5214(03)00706-7.
Kozusko, F., Bourdeau, M., 2007. A unified model of sigmoid tumour growth based on cell proliferation and quiescence. *Cell Prolif.* 40 (6). https://doi.org/10.1111/j.1365-2184.2007.00474.x.
Lu, D.Y., Chen, E.Y., Wong, D.J., Yamamoto, K., Protack, C.D., Williams, W.T., Assi, R., Hall, M.R., Sadaghianloo, N., Dardik, A., 2014. Vein graft adaptation and fistula maturation in the arterial environment. *J. Surg. Res.* 188 (1). https://doi.org/10.1016/j.jss.2014.01.042.
Marks, D.S., Vita, J.A., Folts, J.D., Keaney, J.F., Welch, G.N., Loscalzo, J., 1995. Inhibition of neointimal proliferation in rabbits after vascular injury by a single treatment with a protein adduct of nitric oxide. *J. Clin. Investig.* 96 (6). https://doi.org/10.1172/JCI118328.
Marušic, M., Bajzer, Ž., Vuk-Pavlovic, S., Freyer, J.P., 1994. Tumor growth in vivo and as multicellular spheroids compared by mathematical models. *Bull. Math. Biol.* 56 (4). https://doi.org/10.1007/BF02460714.
Meirson, T., Orion, E., Di Mario, C., Webb, C., Patel, N., Channon, K.M., Ben Gal, Y., Taggart, D.P., 2015. Flow patterns in externally stented saphenous vein grafts and development of intimal hyperplasia. *J. Thorac. Cardiovasc. Surg.* 150 (4). https://doi.org/10.1016/j.jtcvs.2015.04.061.
Model, L. S., & Dardik, A. (2012). Neointimal Hyperplasia: Basic Considerations. In *Haimovici's Vascular Surgery: 6th Edition*. 10.1002/9781118481370.ch10.
Muto, A., Model, L., Ziegler, K., Eghbalieh, S.D.D., Dardik, A., 2010. Mechanisms of vein graft adaptation to the arterial circulation - Insights into the neointimal algorithm and management strategies. *Circ. J.* 74 (8). https://doi.org/10.1253/circj.CJ-10-0495.
Ninno, F., Tsui, J., Balabani, S., Diaz-Zuccarini, V., 2023. A systematic review of clinical and biomechanical engineering perspectives on the prediction of restenosis in coronary and peripheral arteries. *JVS-Vascular Science*. https://doi.org/10.1016/j.jvssci.2023.100128.
Ninno, F., Chiastra, C., Colombo, M., Dardik, A., Strosberg, D., Aboian, E., Tsui, J., Bartlett, M., Balabani, S., Díaz-Zuccarini, V., 2024. Modelling lower-limb peripheral arterial disease using clinically available datasets: impact of inflow boundary conditions on hemodynamic indices for restenosis prediction. *Comput. Methods Programs Biomed.* 251. https://doi.org/10.1016/j.cmpb.2024.108214.
Nishio, E., Fukushima, K., Shiozaki, M., Watanabe, Y., 1996. Nitric oxide donor SNAP induces apoptosis in smooth muscle cells through cGMP-independent mechanism. *Biochem. Biophys. Res. Commun.* 221 (1). https://doi.org/10.1006/bbrc.1996.0563.
Owens, C.D., 2010. Adaptive changes in autogenous vein grafts for arterial reconstruction: Clinical implications. *J. Vasc. Surg.* 51 (3). https://doi.org/10.1016/j.jvs.2009.07.102.
Owens, C.D., Gasper, W.J., Rahman, A.S., Conte, M.S., 2015. Vein graft failure. *J. Vasc. Surg.* 61 (1). https://doi.org/10.1016/j.jvs.2013.08.019.
Palumbo, R., Gaetano, C., Antonini, A., Pompilio, G., Bracco, E., Rönnstrand, L., Heldin, C.H., Capogrossi, M.C., 2002. Different effects of high and low shear stress on platelet-derived growth factor isoform release by endothelial cells: Consequences for smooth muscle cell migration. *Arterioscler. Thromb. Vasc. Biol.* 22 (3). https://doi.org/10.1161/hq0302.104528.
Pearce, C.G., Najjar, S.F., Kapadia, M.R., Murar, J., Eng, J., Lyle, B., Aalami, O.O., Jiang, Q., Hrabie, J.A., Saavedra, J.E., Keefer, L.K., Kibbe, M.R., 2008. Beneficial effect of a short-acting NO donor for the prevention of neointimal hyperplasia. *Free Radic. Biol. Med.* 44 (1). https://doi.org/10.1016/j.freeradbiomed.2007.09.010.
Plata, A.M., Sherwin, S.J., Krams, R., 2010. Endothelial nitric oxide production and transport in flow chambers: The importance of convection. *Ann. Biomed. Eng.* 38 (9). https://doi.org/10.1007/s10439-010-0039-x.
Ponzini, R., Vergara, C., Redaelli, A., Veneziani, A., 2006. Reliable CFD-based estimation of flow rate in haemodynamics measures. *Ultrasound Med. Biol.* https://doi.org/10.1016/j.ultrasmedbio.2006.05.022.
Reisig, K., Clyne, A.M., 2010. Fibroblast growth factor-2 binding to the endothelial basement membrane peaks at a physiologically relevant shear stress. *Matrix Biol.* 29 (7). https://doi.org/10.1016/j.matbio.2010.07.003.
Schwartz, R.S., Holmes, D.R., Topol, E.J., 1992. The restenosis paradigm revisited: An alternative proposal for cellular mechanisms. *J. Am. Coll. Cardiol.* 20 (5). https://doi.org/10.1016/0735-1097(92)90389-5.
Silva, T., Jäger, W., Neuss-Radu, M., Sequeira, A., 2020. Modeling of the early stage of atherosclerosis with emphasis on the regulation of the endothelial permeability. *J. Theor. Biol.* 496. https://doi.org/10.1016/j.jtbi.2020.110229.
Singh, M., Gersh, B.J., McClelland, R.L., Ho, K.K.L., Willerson, J.T., Penny, W.F., Holmes, D.R., 2004. Clinical and angiographic predictors of restenosis after percutaneous coronary intervention: Insights from the Prevention of Restenosis with Tranilast and Its Outcomes (PRESTO) trial. *Circulation* 109 (22). https://doi.org/10.1161/01.CIR.0000131898.18849.65.
Vesti, B.R., Primozich, J., Bergelin, R.O., Strandness, E., 2001. Follow-up of valves in saphenous vein bypass grafts with duplex ultrasonography. *J. Vasc. Surg.* 33 (2). https://doi.org/10.1067/mva.2001.111744.
Walpole, J., Papin, J.A., Peirce, S.M., 2013. Multiscale computational models of complex biological systems. *Annu. Rev. Biomed. Eng.* 15. https://doi.org/10.1146/annurev-bioeng-071811-150104.
Zain, M. A., Jamil, R. T., Siddiqui, W. J., 2022, January. *Neointimal Hyperplasia*. In: StatPearls [Internet]. Treasure Island (FL): StatPearls Publishing.